Effect on passivating molecule and antisolvent on lifetime of green Dion-Jacobson perovskite light-emitting diodes

Xinshun Qin,[1] Yanling He,[1] Chun Ki Tao,[2] Aleksandr Sergeev,[2] Kam Sing Wong,[2] Zhilin Ren,[1] Qiong Liang,[3] Tiklun Leung,[4] Gang Li,[3] Jasminka Popović,[5] Alan Man Ching Ng,[6] and Aleksandra B. Djurišić[1,*]

[1] Department of Physics, The University of Hong Kong, Pokfulam Road, Hong Kong

[2]Department of Physics, The Hong Kong University of Science and Technology, Clearwater Bay, Hong Kong.

[3]Dept. of Electronic and Information Engineering, The Hong Kong Polytechnic University, 11 Yuk Choi Rd, Hung Hom, Hong Kong

[4] School of Physics, The University of Sydney, Sydney, NSW, 2006 Australia

[5]Ruđer Bošković Institute, Bijenička 54, 10000 Zagreb, Croatia

[6]Core Research Facilities, Southern University of Science and Technology, No. 1088, Xueyuan Rd., Shenzhen, 518055, Guangdong, PR China.

ABSTRACT: We investigated the influence of two passivating molecules containing P=O group on the performance of quasi-2D Dion-Jacobson halide perovskite light emitting diodes, namely triphenylphosphine oxide (TPPO) and diphenyl-4-triphenylsilylphenyl phosphine oxide (TSPO1). We found that both passivating molecules lead to increased efficiency compared to control devices, while they had opposite effects on device lifetime, with decrease observed for TPPO and increase observed for TSPO1. The two passivating molecules resulted in differences in energy level alignment, electron injection, film morphology and crystallinity, and ion migration during operation. While TPPO resulted in improved photoluminescence decay times, overall higher maximum external quantum efficiency (EQE) and device lifetime are obtained for TSPO1 compared to TPPO (14.4% vs. 12.4% EQE, 341 min. vs. 42 min T_{50}).

Keywords: lead halide perovskite, LED, passivation, stability, lifetime

INTRODUCTION

2D metal halide perovskites have been attracting increasing attention for application in various optoelectronic devices.[1-3] There are two main groups of 2D perovskites, Ruddlesden-Popper (RP) and Dion-Jacobson (DJ) materials. RP perovskites contain a bilayer of monovalent organic cations separating the layers of corner-sharing lead halide octahedra, while DJ perovskites have a single layer of diammonium cations, resulting in stronger bonding between the layers (as the organic cation bilayer in RP perovskites is bound by weak van der Waals forces) and improved out of plane charge transport.[3,4] RP perovskites have the formula $C_2A_{n-1}M_nX_{3n+1}$, where C is the monovalent bulky spacer cation, A is a small monovalent organic cation or Cs^+, M is a divalent metal cation (Pb^{2+} or Sn^{2+}), X is a halide anion, and *n* is the number of octahedral layers, while DJ perovskites have the formula $DA_{n-1}M_nX_{3n+1}$, where D is divalent spacer cation.[2,3] Due to their promising properties, interest in DJ halide perovskites has been rising, resulting in rapid advances in their device applications. While these materials have been more frequently used in solar cells, where they demonstrated stability advantage over RP perovskites,[1-3] there is also interest for their application in light-emitting diodes (LEDs) However, progress in their LED applications has been slower compared to solar cells, which is not entirely unexpected since these materials are more recent, and their efficiency still lags behind record results for RP perovskite LEDs. Nevertheless, DJ perovskite LEDs emitting in near-infrared (NIR),[5,11,13] green,[6-8,12,14] and blue[9,10] spectral ranges have been reported, with the reported efficiencies in the blue spectral range of 2.65%[10] and 8.5%,[9] while for green spectral range wider ranging values were reported, such as 1.06%,[7] 8.5%,[14] 10.5%,[12] 12.85,[8] and 17.1%.[6]

While their structure (stronger bonding and shorter interlayer spacing) is expected to result in increased stability[2] and direct comparisons of RP and DJ perovskite-based LEDs indeed confirmed stability advantage of DJ LEDs,[5] the stability advantage, if any, is less clear for the devices operating in the visible spectral range. The reported lifetimes for NIR-based DJ perovskites are indeed long (100 h[5] and 189.4 h[11]), but the reported lifetimes of visible LEDs range are significantly smaller, 2 min.[10] to 3.6 min.[9] for blue, and ~15 min.[14] to 70 min.[8] for green. Thus, further progress is needed in both efficiency and stability, in particular for devices in the visible spectral range, to reach performance records of RP perovskites. To achieve this goal, it is necessary to have better understanding of crystallization of these materials to be able to achieve improved phase composition control, as well as understanding of defects and their passivation, all of which have been considerably more extensively studied for RP perovskites. Nevertheless, basic principles, i.e., the non-radiative defects passivation, balance hole and electron injection, and favorable for energy funneling phase-composition are applicable to both materials. The last requirement is specific to quasi-2D perovskites, as the solution processable films with n>1 typically contain different phases, i.e. domains with different *n*.[1,3] These domains have different bandgaps and exciton binding energies (increasing as *n* decreases), and the material typically exhibits energy transfer from lower *n* (higher bandgap) to higher *n* (lower bandgap) phase, so called energy funneling.[3] The phase composition of the film is strongly depends on the solution composition and the deposition condition details which affect the crystallization of the film.

Crystallization kinetics and consequently phase distribution can be controlled by the choice of solvent,[2] antisolvents, and additives.[6] The use of additives is particularly interesting, since the additives can not only regulate crystallization and tune phase distribution, but also affect the film morphology and passivate defects to improve efficiency.[6] Different additives have been reported to date for DJ-based LEDs,[6,8,9,12,14] and even wider range of additives has been reported for other types of perovskite materials and/or perovskite devices.[15-26] The effects of these various additives on the film properties and device efficiency have been thoroughly investigated, but the effect of additives on lifetime has attracted comparatively less attention beyond the obvious attribution of improved lifetimes to defect passivation, since commonly fewer defects=reduced ion migration=improved lifetime and simultaneous improvements in both efficiency and lifetime are observed.[18,25,26] However, we have previously observed that while triphenylphosphine oxide (TPPO) passivation improved efficiency (from 9.41% to 12.85%), it significantly worsened the lifetime (from 70 min. to 13 min.).[8] Considering the fact that phosphine oxide additives are widely used due to effectiveness of P=O bond in passivating uncoordinated Pb^{2+}, it is important to understand possible effects of such additives on both efficiency and stability in order to design more effective passivation molecules. In addition, it has been recently proposed that 2,7- bis(diphenylphosphoryl)-9,9′-spirobifluorene (SPPO13) improves performance compared to TPPO since it can not only passivate the defects, but also promote electron injection into the perovskite layer, in contrast to low-conductive TPPO.[24] Thus, we have selected diphenyl-4-triphenylsilylphenyl phosphine oxide (TSPO1), which has been used as electron transport layer (ETL) in organic light emitting diodes[27] as a passivating molecule and investigated the performance of TSPO1 vs. TPPO passivated perovskite LEDs. Since both molecules have a single P=O bond, their comparison is expected to provide improved understanding of the relative effects of defect passivation vs. electron injection efficiency on the performance of perovskite LEDs. Due to differences in solubility of TPPO and TSPO1, two different solvents were used. We have found that the solvent used affects the performance, but the

comparison trends between TPPO and TSPO1 remain the same for two solvents, with TPPO passivation resulting in worsening of the lifetime compared to control (no passivation) device, while TSPO1 passivation resulted in the improvement of the lifetime compared to control device. Reasons responsible for the observed behavior are discussed.

RESULTS AND DISCUSSION

Figure 1 a-c and **Figure S1** show the absorption spectra, photoluminescence (PL) spectra, and X-ray diffraction (XRD) patterns for different passivation molecules/solvents of the DJ perovskite emitting layer. The control devices do not use any antisolvent as we use vapor annealing process[8,28] to obtain DJ perovskite emitting layer with bright luminescence. The use of passivating molecule requires the use of antisolvent, as the passivating molecule, such as TPPO, is commonly dissolved into antisolvent and applied during antisolvent treatment. Different solvents have been used for TPPO in the literature, such as chloroform,[22,25,26] methyl acetate (MeOAc),[8,15] and toluene (Tol).[21] TSPO1 is commonly deposited by vacuum evaporation,[27] and the supplier of the chemical lists toluene as possible solvent. As we have previously observed increasd efficiency but reduced lifetime for TPPO in MeOAc,[8] we have selected MeOAc as one of the conditions to study reasons for this unexpected phenomenon. However, TSPO1 has poor solubility in MeOAc (requires stirring for two days to dissolve), and therefore we have also included a comparison of TPPO and TSPO1 in Tol. Since the antisolvent used affects the perovskite film properties,[29] we have also examined the use of MeOAc and Tol antisolvents without passivating molecules. In the absorption spectra, we can observe peaks corresponding to lower *n* phases, usual for DJ perovskite materials, since higher *n* phases (n>3) have higher formation enthalpy.[12,14] We can also observe that the passivating molecules and/or solvents used do not have a significant effect on the distribution of the different *n* phases in the films. While it was previously reported that TPPO could affect crystallization of the perovskite and suppress the formation of low *n* phases[21,25] or the formation of bulk phase,[22] no such effects were observed in this work. Thus, the effect of TPPO on changing the *n* phase distribution, if any, is likely dependent on the composition of the perovskite and it does not contribute significantly to the behavior observed in this work for 1,6-hexanediammonium (HDA) - 1,10-Decanediammonium (DDA) based cesium lead bromide perovskite. However, from the ratio of diffraction lines vs. background intensity, we observe an evident decrease in crystallinity of the films after TPPO passivation compared to control and TSPO1. Reduced crystallinity was also previously reported for 3D perovskite with TOPO additive,[23] but there have been no reports of reduced crystallinity of quasi-2D perovskite after TPPO passivation.

Despite reduced crystallinity of TPPO samples, we observe the enhancement of the PL intensity for both passivating molecules, which is consistent with defect passivation,[22] although in the case of TPPO it is possible that confinement to smaller size crystals can also enhance the emission.[23] However, it should be noted that PL intensity is a result of a complex interplay between radiative and non-radiative recombination rates, which are affected by crystal size (smaller size leads to increased radiative rate) and trap density (increased surface area implies more traps, and more traps lead to increased non-radiative recombination; trap passivation would lead to reduced non-radiative recombination. This is further complicated by energy transfer between different *n* phases in the film, which is dependent on the film microstructure. From line broadening analysis performed on the 002 *n*=2 diffraction lines showed that coherent crystallite domains in the case of TPPO amount to ~ 11 nm while control and TPSO samples contain crystallites with sizes ~ 20 nm.

The effect of passivation on the device performance was also investigated (schematic diagram of the device architecture and structure of passivating molecules are shown in **Figure S2**, while molecular structures of HDA and DDA, as well as that of DJ perovskite are shown in **Figure S3**), and the obtained results are summarized in **Table 1** and shown in **Figure 2** and **Figure S4**. The devices exhibit significant differences in performance, while EL spectra in all cases show excellent spectral stability, as illustrated in **Figure S5**. From the morphology of the films, shown in **Figures S6** and **S7**, we can observe that films with passivation molecules dissolved in MeOAc exhibit increase in grain size (solvent only) and appearance of large aggregates (MeOAc with passivating molecule), while the films with Tol-based passivation exhibit similar morphology to control samples, although occasionally large aggregates are present in these samples as well. Re-crystallization of the samples can occur upon rinsing with antisolvent,[30] and we can indeed observe an increase in PL intensity and maximum luminance of the devices with two antisolvents. There is no significant difference between the best efficiency achieved for control device and those prepared with MeOAc and Tol, but there is a drop in average efficiency with Tol. Device lifetime shows a small reduction with the use of antisolvent, which is more pronounced with MeOAc compared to Tol. For TSPO1 passivation, significantly better performance is observed for Tol compared to MeOAc, which is likely due to better solubility of TSPO1 in Tol. For both antisolvents, significantly longer lifetime is obtained compared to control devices. For TPPO passivation, we observe higher efficiency and lower lifetime for MeOAc compared to Tol, with the difference in lifetime significantly higher compared to difference in efficiency. Since the absorption, XRD, and PL do not appear to have any dependence on the solvent used, we will examine more closely the devices with TPPO in MeOAc and TSPO1 in Tol as they exhibit the highest efficiencies. At the same time, they also exhibit the largest difference in device lifetimes. This could be in part due to aggregates observed on the film surface for TPPO in MeOAc (increased surface defects could lead to microscopic shorts and shorter lifetime). As a result, the device lifetime shortening is the general feature of TPPO passivation in our work. Some reduction of the device lifetime is observed for MeOAc compared to Tol for all three conditions (control, TPPO, TSPO1), but passivating molecule has a more significant effect on the lifetime, with TPPO-passivated devices in all cases exhibiting shorter lifetime compared to control devices while TSPO1-passivated devices exhibit longer lifetime.

To examine the passivation effects of TPPO and TSPO1, we performed Fourier transform infrared (FTIR) spectroscopy measurements (**Figure S8)**. Both molecules possess P=O groups which are expected to passivate uncoordinated Pb^{2+}. MeOAc does not affect the FTIR spectra significantly, but Tol does cause some small changes in the 600-1100 cm^{-1} region, which likely originate from the traces of solvent due to higher boiling point of toluene (~110ºC, compared to ~57ºC for MeOAc). In TPPO passivated samples, we can observe clear presence of P=O stretching vibration at ~1175 cm^{-1},[22,25,26] which is more pronounced for TPPO in MeOAc compared to TPPO in Tol. Similar observation applies to a peak at ~542 cm^{-1}, attributed to Pb-O vibration,[19] as well as peaks at ~722 cm^{-1} and ~696 cm^{-1}, with the former attributed to P=O:Pb interaction.[26] In TSPO1 passivated samples, a peak at ~1111 cm^{-1} is observed instead of ~1175 cm^{-1}, and we also observe peaks at 699 cm^{-1} and 568 cm^{-1}. Similar to TPPO, peaks for TSPO1 in MeOAc are more pronounced compared to TSPO1 in Tol. The peak shifts observed indicate differences in the interaction between Pb^{2+} and P=O for the two passivating molecules. One possible reason for the observed differences is reduced crystallinity of TPPO-passivated films, which could result in differences in types of defects present in the samples. The peaks related to P=O and P=O:Pb interactions are more pronounced in TPPO-passivated samples compared to TSPO1 passivation, in agreement with increased PL decay time, as shown in **Figure 1d** and summarized in **Table S1**, based on biexponential decay model of time resolved photoluminescence (TRPL) curves commonly used for halide perovskites.[6,14] Increased PL lifetime with TPPO passivation is in agreement with previous reports.[22] However, based on the trends observed in TRPL one would expect increased EQE of TPPO-passivated devices compared to TSPO1-passivated ones. Thus, it is necessary to examine defect passivation by TPPO and TSPO1 more closely. Possible reasons for mismatch in trends between PL and TRPL measurements and EQE are differences in electron injection/electron transport. Another possible reason is charge transfer between perovskite and TSPO1. Longer lifetime was previously reported for TPPO passivated samples compared to SPPO13 passivated samples, which was attributed to charge transfer between the perovskite and SPPO13, compared to no charge transfer to insulating TPPO.[24] Since TSPO1 is also an ETL material, there is a possibility of charge transfer similar to SPPO13 case.

To examine defect passivation and charge transport effects of the two molecules in more detail, we performed space charge limited current (SCLC) characterization for electron-only and hole-only devices, as shown in **Figure 3a** and **b** and summarized in **Table S1**, and examined energy level alignment using UPS, as shown in **Figure 4**. After determining the trap filled limit voltage V_{TFL} from SCLC curves, the trap density N_t can be determined as:[6,19]

$$N_t = \frac{2\varepsilon\varepsilon_0 V_{TFL}}{eL^2}$$

where *L* is the thickness of the perovskite film (~30 nm), *e* is the elementary charge (1.602×10^{-19} C), ε is the relative dielectric constant (ε=25),[31,32] and ε_0 is the vacuum permittivity (8.8542×10^{-14} F/cm). It should be noted that SCLC data can provide information on trends in trap densities with different passivating molecules with all other factors kept constant. However, since device architecture for hole-only devices and electron-only devices is inevitably different from an actual device due to solution-processing related constraints, differences in actual trap concentrations and hole and electron currents between single charge carrier and actual devices are expected. From the obtained SCLC data, we can observe improved reduction of the N_t for TSPO1 passivation compared to TPPO passivation. Both passivating molecules reduce the density of hole traps, while for TSPO1 we observe comparable electron trap density, and an increase in electron trap density for TPPO compared to control samples. The decrease in trap density in hole-only devices indicates that both molecules exhibit trap passivation, consistent with the observed increase in EQE, and it

points toward the possibility that reduced PL decay time in TSPO1 passivated samples compared to TPPO is because of charge transfer. From the energy level diagrams obtained from UPS measurements shown in **Figure 4**, we can observe that TPPO passivation results in a significant vacuum level shift, which does not occur for TSPO1. The presence of a large vacuum level shift (> 0.5 eV) has been attributed to the formation of interfacial dipoles in organic materials.[33] The presence of a dipole affects the energy level alignment in the device, charge distribution and the barriers for charge injection.[34] Thus, low conductivity of TPPO results in the presence of interfacial dipoles, which affects the barriers for charge injection and consequently the device performance. Surface dipoles could also in part originate from the dipole moment of the molecule, as the total shift of the work function at the interface represents the sum of contributions from interface dipoles (arising from charge redistribution at the interface), possible geometry relaxation of the surface after modification (usually small contribution), and the molecular dipole moment.[35] Polar P=O group in phosphine oxide compounds has a dipole moment,[36,37] which is dependent on the structure of the molecule.[37] TPPO has a large dipole moment of 3.27 D,[37] while dipole moment for TSPO1 has not been reported. To further examine any changes in surface potential of the films for different passivation, Kelvin probe force microscopy (KPFM)[38] was performed, as shown in **Figure S9.** We can observe that surface passivation results in a change of the surface potential. The widest range of surface potential variation across scanned area observed for TPPO indicating low uniformity of surface potential, while the smallest range was observed for TSPO1. The average surface potential changes from 16.1 mV for control to 28.1 mV for TPPO and 10.4 mV for TSPO1, indicating that passivating molecules can affect the surface potential, and that observed change is more pronounced for TPPO, in agreement with UPS results.

The presence of surface dipoles is not necessarily detrimental for the efficiency, since high brightness was previously observed for passivated interfaces despite unbalanced injection and increased leakage current,[23] likely due to nonradiative defect passivation. However, the presence of dipoles could potentially cause detrimental effects on device lifetime due to accumulation of charges, as it is known that excess charges,[39,40] in particular hole excess,[40] are detrimental to the perovskite stability. We indeed observe significant reduction in the device lifetime with TPPO passivation, as shown in **Figure 3c** and **Table 1** and in agreement with our previous work,[8] but different from reports on TPPO passivation of Ruddlesden-Popper quasi-2D perovskite materials.[25,26] In those materials, reduced degradation was attributed to edge passivation, suppression of the generation of superoxide ions, and reduced ion migration.[26] We have therefore examined differences in ion migration for TPPO and TSPO1 passivation from secondary ion mass spectroscopy (SIMS) measurements, as shown in **Figure 5**. We can observe that there is more pronounced ion migration in TPPO-passivated devices, with increased migration observed for Cs^+ (small effect), as well as Br^- and Al^-. The movement of bromide towards the metal electrode occurs simultaneously with the movement of Al^- towards ITO electrode. Ion migration is a common cause of degradation in perovskite LEDs,[41] and the migration for all elements investigated here is less pronounced in TSPO1-passivated devices. To examine reasons for differences in the ion migration, we examined the interaction between passivating molecules and perovskite precursors CsBr, $PbBr_2$, and $DDABr_2$ using performed nuclear magnetic resonance (NMR) measurements, as shown in **Figure 6.** It can be observed that TPPO exhibits strongest interaction with the organic cation and the weakest interaction with Cs^+, in agreement with other literature reports.[21,24,25] Different from SPPO13,[24] we do not observe stronger interactions of the passivating molecule TSPO1 with Cs^+, or any other cation compared to TPPO, in agreement with FTIR results where peaks related to P=O and P=O:Pb interactions are more pronounced for TPPO passivation. Therefore, we cannot attribute reduced ion migration during the operation to better passivating effects of TSPO1. Thus, possible reason is reduced crystallinity of TPPO sample, as this would lead to more grain boundaries. Grain boundaries represent major pathways for ion migration,[42-45] since higher ionic diffusivity in grain boundaries results in faster ion migration compared to the bulk.[42] Therefore, transmission electron microscopy (TEM) imaging of the control and passivated films was performed, as shown in **Figure 7**. The average grain sizes in control, TPPO-, and TSPO1-passivated samples are 28 nm, 22 nm, and 31 nm, respectively. The trend in grain sizes follows the observed trend in device lifetimes. To further examine the hypothesis that reduced crystallinity of TPPO sample and resulting increase in grain boundaries leads to increased ion migration and reduced lifetime, we have also attempted different passivating conditions for TPPO in MeOAc to try to obtain improved crystallinity, and for reduced concentration of TPPO we have indeed obtained an increase in XRD peak corresponding to 002 n=2 diffraction and increased average particle size, as shown in **Figure S10**. The device performance is summarized in **Table 1** and illustrated in **Figure S11**. We can observe a small improvement in the best EQE obtained, and a significant improvement in the device lifetime compared to standard condition for TPPO in MeOAc, although none of the TPPO passivated samples exhibit improved lifetime compared to control samples. The obtained results indicate that grain size and grain boundaries play an important role in device stability. Passivating molecules which do not facilitate surface recrystallization, such as TSPO1, thus may be preferrable to small passivating molecules such as TPPO.

CONCLUSIONS

We have investigated the effect of two P=O based passivating molecules, TPPO and TSPO1, on the performance of PeLEDs. We found that both passivating molecules enhanced the maximum EQE (10.9 % for control, 12.4% for TPPO passivation, 14.4% for TSPO1 passivation), but had the opposite effect on device lifetime. Reduction of T_{50} lifetime from 105 min. (control) to 42 min. was observed for TPPO passivation, while an increase to 341 min. was obtained for TSPO1. The significant ion migration was found in TPPO-passivated devices. Observed differences in ion migration and consequently device lifetime are attributed to reduced crystallinity after TPPO passivation, resulting in increase in grain boundaries which facilitate ion migration, as well as less favorable energy level alignment compared to TSPO1. Our work highlights the need to examine effects of recrystallization after passivation (affected both by antisolvent used as well as passivating molecule) and the important role of grain boundaries in device lifetime.

ASSOCIATED CONTENT

Supporting Information. Absorption and PL spectra, XRD patterns, J-L-V curves and EQE for additional conditions, device diagram, chemical formulae of TPPO and TSPO1, EL spectra, SEM images, FTIR spectra, KPFM images, SIMS results, SCLC and TRPL fitting parameters. This material is available free of charge via the Internet at http://pubs.acs.org.

AUTHOR INFORMATION

Corresponding Authors

Aleksandra B. Djurišić: dalek@hku.hk

Author Contributions

X. S. Qin conducted LED fabrication and characterization experiments, collected and summarized the experimental data. A. B Djurišić designed the whole study, analyzed and interpreted results and wrote the manuscript. Q. Liang and G. Li were responsible for XRD experiment. J. Popović analyzed XRD data. Y. He conducted the NMR, UPS, TEM, KPFM, and SIMS experiments, and data analysis was performed by Y. L. He and A. M. C. Ng (UPS, SIMS, TEM) and T. L. Leung (NMR). C. K. Tao, A. Sergeev and K. S. Wong were responsible for PL and TRPL measurements. All co-authors provided input to the final version of the manuscript.

Notes

The authors declare no competing financial interest.

ACKNOWLEDGMENT

This work was supported by the NSFC project 6207032617, RGC GRF project 17301520, RGC CRF project 7035-20G, Seed Funding for Basic Research and Seed Funding for Strategic Interdisciplinary Research Scheme of the University of Hong Kong, and the PZS-2019-02-2068 project financed by the *"Research Cooperability"* Program of the Croatian Science Foundation and European Union from the European Social Fund under the Operational Programme Efficient Human Resources 2014-2020. The authors would like to thank Ms. Ren Zhanying from Core Research Facilities of SUSTech for her help with the NMR measurements.

EXPERIMENTAL SECTION

Materials. Lead(II) bromide ($PbBr_2$, 98%), cesium bromide (CsBr, 99.999%), and [2-(9H-Carbazol-9-yl)ethyl]phosphonic Acid (2PACz, 98%) were purchased from TCI. 1,10-Decanediammonium dibromide ($DDABr_2$), 1,6-hexanediammonium dibromide ($HDABr_2$), and poly[(9,9-dioctylfluorenyl-2,7-diyl)-alt-(4,4'-(N-(4-butylphenyl)))] (TFB) were purchased from Xi'an Polymer Light Technology Corporation. Triphenylphosphine oxide (TPPO, 99%) and methyl acetate (MeOAc, >99%) were purchased from Acros Organics. Dimethyl sulfoxide (DMSO, anhydrous, 99.9%), chlorobenzene (CB, anhydrous, 99.8%) and 85% H_3PO_4/D_2O were purchased from Sigma-Aldrich. Toluene (99.85%) was purchased from Thermo scientific. 2-propanol (anhydrous, 99.5%) was purchased from Alfa Aesar. DMSO-d6 was purchased from J&K Scientific.1,3,5-tris(1-phenyl-1H-benzimidazol-2-yl)benzene (TPBi, > 99.8%), 8-hydroxyquinolinolato-lithium (Liq, >99.9%), and diphenyl-4-triphenylsilylphenyl-phosphine oxide (TSPO1, >99%) were purchased from Luminescence Technology Corporation. Aluminum pellets (Al, 99.999%) were purchased from Kurt J. Lesker Company. All materials were directly used as received.

Fabrication of perovskite thin films. The $DDA_{0.75}HDA_{0.25}Cs_3Pb_4Br_{13}$ perovskite was synthesized by the method reported previously.[8] Briefly, precursor solution was prepared by dissolving $DDABr_2$, $HDABr_2$, CsBr and $PbBr_2$ in DMSO with the molar ratio of 0.75:0.25:4:4. The concentration of the solution as determined by Pb^{2+} is 0.2 M. 20 mL of DMSO was added in a Petri dish (diameter 60 mm, with lid) at least 10 min before use. The precursor solution was spin coated on the substrate at 5000 rpm for 35 s. The substrate was then placed at the center of the Petri dish covered with the lid and kept inside for 90 s to complete the vapor annealing process. For the passivated perovskite films, TSPO1/TPPO was dissolved in toluene and methyl acetate at a concentration of 1 mg mL^{-1}, respectively. Due to lower solubility of TSPO1, solution for TSPO1 in Tol was stirred for one day, while solution of TSPO1 in MeOAc was stirred for two days before use. TPPO was readily soluble in both MeOAc and Tol, and in addition to concentration of 1 mg mL^{-1}, 0.5 mg mL^{-1} solution was also prepared. After the vapor annealing process, TSPO1/TPPO solution was deposited onto the perovskite film during the spinning at 5000 rpm for 35 s.

Fabrication of perovskite LED devices. Patterned ITO/glass substrates were cleaned by sonication in Decon 90, deionized water, acetone, toluene, acetone, and ethanol in sequence, followed by oxygen plasma treatment before use. The 2PACz solution (0.75 mg mL^{-1} in 2-propanol) was spin-coated on cleaned ITO/glass substrates at 4000 rpm for 30 s inside an Ar-filled glove box, followed by annealing at 100 ºC for 10 min. A TFB thin layer was prepared on top of the 2PACz film by spin coating of TFB solution in chlorobenzene at a concentration of 10 mg mL^{-1}, followed by annealing at 120 ºC for 30 min. The TFB thin film was subjected to oxygen plasma for 10 s before proceeding with perovskite deposition. Perovskite thin films were then deposited following the procedures described above. The substrates were transferred to the thermal evaporator for thermal deposition of TPBi (40 nm), Liq (2 nm), and Al electrode (100 nm) in sequence. The device area was defined by the cross-sectional area of the ITO and Al electrodes as 0.04 cm^2.

Characterization of thin films and devices. Optical absorption spectra were obtained using a Cary 60 UV-Vis Spectrometer (Agilent Technologies). Steady-state PL spectra were measured in ambient from an integrated confocal microRaman system (HORIBA, XploRA PLUS) under a 405 nm laser. The SEM images were investigated using a Hitachi S-4800 FEG Scanning Electron Microscope. ATR-FTIR spectra were obtained from Spectrum Two ATR-FTIR spectrometer (PerkinElmer). GIXRD data were measured using a Rigaku Smartlab 9 kW XRD. Time-resolved photoluminescence (TRPL) was carried out by exciting the sample with a 100 fs laser generated by a mode-locked titanium sapphire oscillator laser with a 76 MHz repetition rate. To achieve a repetition rate longer than the total PL decay time, the output was pulse-picked down to 745 kHz, providing a 1.34-µs distance between sequential pulses. After pulse-picking, a residual pulse with a two-orders-lower amplitude and 21.5-ns distance from the main pulse appears (Fig. 1d). The effect of the residual pulse on calculated PL decay values was accounted for by re-convolution of the raw PL decay data with an instrument response function (IRF) of the TCSPC setup. The oscillator was tuned to 840 nm, and the output was frequency doubled to 420 nm using a beta barium borate (BBO) crystal. The beam was attenuated by a variable ND wheel and the power before the sample was measured with a laser power meter (Newport 2936R). The laser was focused onto the sample and the photoluminescence is collected into a monochromator (Acton Spectrapro 275) by a pair of achromatic lenses. The peak wavelength of the PL was dispersed by a 1200 l/mm grating onto a photon counter and time correlated single photon counting is carried out using a Becker and Hickl system. The UPS spectra were obtained using an ESCALAB 250xi from Thermo Fisher equipped with a helium discharge lamp with energies of 21.22 eV. A bias voltage of−10 V was applied for each sample during UPS measurements to obtain an accurate secondary electron cut-off. The ^{31}P NMR spectra of TPPO and TSPO1 were recorded on a Bruker Advance III spectrometer using DMSO-d6 as the solvents and referenced to phosphoric acid (85% H_3PO_4 / D_2O) as standard. ToF-SIMS spectra was applied to interpret the surface structure and element distribution by PHI nano TOF II with TRIFT analyzer. Ar ion source with 3 keV energy, primary current of 30 nA and primary ion dose of 400x400 ions/μm^2 was used for both negative and positive mode sputtering. The morphology and crystallite size of the samples were obtained by TEM characterization using F30 from FEI. The film samples were scraped inside glovebox and then copper grids were transferred to the vacuum chamber of the TEM. The AFM and KPFM measurements were performed with Bruker MFP-3D Stand Alone in AM-KPFM mode. The samples were grounded and Pt/Ir-coated tips were used during the KPFM measurements. Space-charge-limited current (SCLC) measurement was carried using a computer-controlled Keithley 2400 SourceMeter in the dark at room temperature. The LED device performance of the perovskite LEDs was characterized using a measurement setup consisting of a programmable Keithley 2400 SourceMeter and a Photoresearch PR-670 spectroradiometer with SL-1X close-up lens. The device lifetime was measured by monitoring the luminescence change of the device under a constant current bias.

REFERENCES

1. Li, Z.; Sun, C. J.; He, T. W.; Jiang, Y. Z.; Wei, J. L.; Huang, Y. M.; Yuan, M. J. High-Performance Quasi-2D Perovskite Light-Emitting Diodes: from Materials to Devices. *Light: Science & Applications* **2021**, *10*, 61.
2. Zhou, N.; Zhou, H. P. Spacer Organic Cation Engineering for Quasi-2D Metal Halide Perovskites and the Optoelectronic Application. *Small Struct.* **2022**, *3*, 2100232.
3. Guo, W.; Yang, Z.; Dang, J. L.; Wang, M. Q. Progress and Perspective in Dion-Jacobson Phase 2D Layered Perovskite Optoelectronic Applications. Nano Energy 2021, 86, 106129.
4. Shi, Z. F.; Ni, Z. Y.; Huang, J. S. Direct Observation of Fast Carriers Transport along Out-of-Plane Direction in a Dion−Jacobson Layered Perovskite. *ACS Energy Lett.* **2022**, *7*, 984−987.
5. Shang, Y. Q.; Liao, Y.; Wei, Q.; Wang, Z. Y.; Xiang, B.; Ke, Y. Q.; Liu, W. M.; Ning, Z. J. Highly Stable Hybrid Perovskite Light-Emitting Diodes Based on Dion-Jacobson Structure, *Sci. Adv.* **2019**, *5*, eaaw8072.
6. Lian Y. J.; Yang, Y.; Gao, J. L.; Qin, C.C. Efficient Dion-Jacobson PeLEDs via additive engineering. *Org. Electron.* **2022**, *102*, 106443.
7. Chen, C. H.; Li, Z. C.; Xue, Q. F.; Su, Y. A.; Lee, C. C.; Yip, H. L.; Chen, W. C.; Chueh, C. C. Engineering of Perovskite Light-Emitting Diodes Based on Quasi-2D Perovskites Formed by Diamine Cations. *Org. Electron.* **2019**, *75*, 105400.
8. Qin, X. S.; Liu, F. Z.; Leung, T. L.; Sun, W. T.; Chan, C. C. S.; Wong, K. S.; Lidija Kanižaj, L.; Popović, J.; Aleksandra B. Djurišić, A. B. Compositional Optimization of Mixed Cation Dion–Jacobson Perovskites for Efficient Green Light Emission. *J. Mater. Chem. C* **2022**, *10*, 108-114.
9. Liu, Y. Q.; Ono, L. K.; Tong, G. Q.; Zhang, H.; Qi, Y. B. Two-Dimensional Dion−Jacobson Structure Perovskites for Efficient Sky-Blue Light-Emitting Diodes. *ACS Energy Lett.* **2021**, *6*, 908−914.
10. Liu, Y. Q.; Ono, L. K.; Tong, G. Q.; Bu, T. L.; Zhang, H.; Ding, C. F.; Zhang, W.; Qi, Y. B. Liu, Y. Q.; Ono, L. K.; Tong, G. Q.; Zhang, H.; Qi, Y. B. Spectral Stable Blue-Light-Emitting Diodes via Asymmetric Organic Diamine Based Dion–Jacobson Perovskites, *J. Am. Chem. Soc.* **2021**, *143*, 19711-19718.
11. Ngai, K. H.; Wei, Q.; Chen, Z. F.; Guo, X. L.; Qin, M. C.; Xie, F. Y.; Chan, C. C. S.; Xing, G. C.; Lu, X. H.; Chen, J.; Wong, K. S.; Xu, J. B.; Long, M. Z. Enhanced Electrochemical Stability by Alkyldiammonium in Dion–Jacobson Perovskite toward Ultrastable Light-Emitting Diodes. *Adv. Optical Mater.* **2021**, *9*, 2100243.
12. Lian, Y. J.; Yang, Y.; Gao, J. L.; Qin, C. C. Efficient Dion–Jacobson Perovskite Light-Emitting Diodes via Mixed Cation Engineering. *Opt. Lett.* **2022**, *47*, 657-660.
13. Yang, H. J.; Tang, J.; Deng, L. L.; Liu, Z.; Yang, X.; Huang, Z. Q.; Yu, H. M.; Wang, K.; Li, J. P. Improved Highly Efficient Dion–Jacobson type Perovskite Light-Emitting Diodes by Effective Surface Polarization Architecture. *Phys. Chem. Chem. Phys.* **2022**, *24*, 7969-7977.
14. Lian, Y. J.; Yang, Y.; He, L. H.; Yang, X. L.; Gao, J. L.; Qin, C. C.; Niu, L. B.; Yang, X. H.; Enhancing the Luminance Efficiency of Formamidinium-Based Dion- Jacobson Perovskite Light-Emitting Diodes via Compositional Engineering. *ACS Appl. Mater. Interfaces* **2022**, *14*, 1659−1669.
15. Li, X. F.; Tian, Y. T.; Yang, L. Q.; Wang, S. M.;Zhao, L.; Ding, J. Q. *In situ* Interfacial Passivation with an Arylphosphine Oxide and Phosphonate Electron Transporting Layer for Efficient All-Solution- Processed PeQLEDs, *Nanoscale* **2022**, *14*, 17230-17236.

16. Huang, S. H.; Liu, N.;Liu, Z. Z.; Zha n, Z. J.;Hu, Z. P.; Du, Z. X.; Zhang, Z. Y.; Luo, J. J.; Du, J.; Tang, J.; Leng, Y. X. Enhanced Amplified Spontaneous Emission in Quasi-2D Perovskite by Facilitating Energy Transfer, *ACS Appl. Mater. Interfaces* **2022**, *14*, 33842−33849.
17. Mishra, J. K.; Yantara, N.; Kanwat, A.; Furuhashi, T.; Ramesh, S.; Salim, T.; Jamaludin, N. F.; Febriansyah, B.; Ooi, Z. E.; Mhaisalkar, S.; Sum, T. C.; Hippalgaonkar, K.; Mathews, N. Defect Passivation Using a Phosphonic Acid Surface Modifier for Efficient RP Perovskite Blue-Light-Emitting Diodes, *ACS Appl. Mater. Interfaces* **2022**, *14*, 34238−34246.
18. Huang, X. F.; Liu, W.; Wang, W.; Lu, Y.; Dong, J.; Li, Y. Q.; Wei, D.; Qiao, B.; Zhao, S. L.; Xu, Z.; Song, D. D. Improved Phase Purity and Film Quality in Quasi-2D Perovskite Light-Emitting Diodes by an Additive With the Trimethacrylate Group, *RSC Adv.* **2022**, *12*, 3081–3089.
19. Li, W. H.; Lai, X.;Meng, F.; Li, G. Q.; Wang, K.; Kyaw, A. K. K.; Sun, X. W. Efficient Defect-Passivation and Charge-Transfer with Interfacial Organophosphorus Ligand Modification for Enhanced Performance of Perovskite Solar Cells. *Sol. Energy Mater. Sol. Cells* **2020**, *211*, 110527.
20. Zhao, C. Y.; Wu, W. P.; Zhan, H. M.; Yuan, W.; Li, H. X.; Zhang, D. Z.; Wang, D. P.; Cheng, Y. X.; Shao, S. Y.; Qin, C. J.; Wang, L. X. Phosphonate/Phosphine Oxide Dyad Additive for Efficient Perovskite Light-Emitting Diodes, *Ang. Chem. Int. Ed.* **2022**, *61*, e202117374.
21. Jamaludin, N. F.; Yantara, N.; Febriansyah, B.; Tay, Y. B.; Muhammad, B. T.; Laxmi, S.; Swee Sien Lim, S. S.; Sum, T. C.; Mhaisalkar, S.; Mathews, N. Additives in Halide Perovskite for Blue-Light-Emitting Diodes: Passivating Agents or Crystallization Modulators? *ACS Energy Lett.* **2021**, *6*, 4265-4272.
22. Yukta, Chini, K. M.; Ranjan, R.; Satapathi, S. Lewis Base Passivation of Quasi-2D Ruddlesden−Popper Perovskite for Order of Magnitude Photoluminescence Enhancement and Improved Stability, *ACS Appl. Electron. Mater.* **2021**, *3*, 1572−1582.
23. Schmidt, I.; Olthof, S.; Xu, H.; Meerholz, K. Phosphine Oxide Additives for High-Brightness Inorganic Perovskite Light-Emitting Diodes. *Adv. Optical Mater.* **2022**, *10*, 2101602.
24. Li, M. L.; Zhao, Y. P.; Qin, X. Q.; Ma, Q. S.; Lu, J. X.; Lin, K. B.; Xu, P.; Li, Y. Q.; Feng, W. J.; Zhang, W. H.; Wei, Z. H. Conductive Phosphine Oxide Passivator Enables Efficient Perovskite Light-Emitting Diodes. *Nano Lett.* **2022**, *22*, 2490−2496.
25. Ma, D. X.; Lin, K. B.; Dong, Y. T.; Choubisa, H.; Proppe, A. H.; Wu, D.; Wang, Y. K.; Chen, B.; Li, P. C.; Fan, J. Z.;Yuan, F. L.; Johnston, A.; Liu, Y.; Kang, Y. T.; Lu, Z. H.; Wei, Z. H.; Sargent, E. H.; Distribution Control Enables Efficient Reduced-Dimensional Perovskite LEDs. *Nature* **2021**, *599*, 594-598.
26. Quan, L. N.; Ma, D. X.; Zhao, Y. B.; Voznyy, O.; Yuan, H. F.; Bladt, E.; Pan, J.; García de Arquer, F. P.; Sabatini, R.; Piontkowski, Z.; Emwas, A. H.; Todorović, P.; Quintero-Bermudez, R.; Walters, G.; Fan, J. Z.; Liu, M. X.; Tan, H. R.; Saidaminov, M. I.; Gao, L.; Li, Y. Y.; Anjum, D. H.; Wei, N. N.; Tang, J.; McCamant, D. W.; Roeffaers, M. B. J.; Bals, S.; Hofkens, J.; Bakr, O. M.; Lu, Z. H.; Sargent, E. H. Edge Stabilization In Reduced-Dimensional Perovskites, *Nat. Commun.* **2020**, *11*, 170.
27. Chen, Z.; Tian, N. T.; Tao, P.; Chen, S. M.; Ma, D. G.; Wang, L. X.; Wong, W. Y. A Pure Blue Phosphorescent Organic Light-Emitting Diode with an External Quantum Efficiency of Over 30% by Using a Tandem Device Architecture, *Adv. Mater. Interfaces **2022***, *9*, 2200932.
28. Peng, X. F.; He, B. C.; Zheng, H. L.; Su, Z. H.; Li, X. Z.; Ji, L.; Zhang, T.; Chen, L.; Qin, C. C.; Gao, X. Y.; Li, S. B.; Yang, X. H. Suppressed Energy Transfer Loss of Dion−Jacobson Perovskite Enabled by DMSO Vapor Treatment for Efficient Sky-Blue Light-Emitting Diodes, *ACS Energy Lett.* **2023**, *8*, 339−346.
29. Xu, L. B.; Che, S. Y.; Huang, J. Y.; Xie, D. Y.; Yao, Y. X.; Wang, P.; Lin, P.; Piao, H. J.; Hu, H. H.; Cui, C.; Wu, F. M.; Yang, D. R.; Yu, X. G. Towards Green Antisolvent for Efficient $CH_3NH_3PbBr_3$ Perovskite Light Emitting Diodes: A Comparison of Toluene, Chlorobenzene, and Ethyl Acetate, *Appl. Phys. Lett.* **2019**, *115*, 033101.
30. Song, Q.; Liang, C. J.; Zhang, H. M.; Ji, C.; Sun, M. J.; Sun, F. L.; Jing, X. P.; You, F. T.; Lu, Y. W.; He, Z. Q. Additional Organic-Solvent-Rinsing Process to Enhance Perovskite Photovoltaic Performance, *Adv. Electron. Mater.* **2019**, *5,* 1900244
31. Zhang, X.; Yang, T. H.; Ren, X. D.; Zhang, L.; Zhao, K.; Liu, S. (F.) Film Formation Control for High Performance Dion–Jacobson 2D Perovskite Solar Cells, *Adv. Energy Mater.* **2021**, *11*, 2002733.
32. Zheng, Y. T.; Niu, T. T.; Qiu, J.; Chao, L. F.; Li, B. X.; Yang, Y. G.; Li, Q.; Lin, C. Q.; Gao, X. Y.; Zhang, C. F.; Xia, Y. D.; Chen Y. H.; Huang, H. Oriented and Uniform Distribution of Dion–Jacobson Phase Perovskites Controlled by Quantum Well Barrier Thickness, *Solar RRL* **2019**, *3*, 1900090.
33. Hill, I. G.; Mäkinen, A. J.; Kafafi, Z. H. Distinguishing Between Interface Dipoles and Band Bending at Metal/Tris-(8-Hydroxyquinoline) Aluminum Interfaces. *Appl. Phys. Lett.* **2000**, *77*, 1825-1827.
34. Zojer, E.; Taucher, T. C.; Oliver T. Hofmann, O. T. The Impact of Dipolar Layers on the Electronic Properties of Organic/Inorganic Hybrid Interfaces, *Adv. Mater. Interfaces* **2019**, *6*, 1900581.
35. Paniagua, S. A.; Giordano, A. J.; Smith, O'Neil L.; Barlow, S.; Li, H.; Armstrong, N. R.; Pemberton, J. E.; Bredás, J.-L.; Ginger, D.; Marder, S. R., Phosphonic Acids for Interfacial Engineering of Transparent Conductive Oxides *Chem. Rev.* **2016**, *116*, 7117−7158.
36. Agarwala, A.; Kaynan, N.; Zaidiner, S.; Yerushalmi, R. Surface Modification of Metal Oxides by Polar Molecules in a Non-Polar, Polarizable Solvent System, *Chem. Commun.* **2014**, *50*, 5397-5399.
37. Carlson, R. D.; Meek, D. W. Dipole Moments of Several Tertiary Phosphine Oxides, Sulfides, and Selenides and of Some Tertiary Arsine Oxides and Sulfides, Inorg. Chem. 1974, 13, 1741-1747.
38. Lin, Z. H.; Chang, J. J.; Xiao, J. X.; Zhu, H.; Xu, Q. H.; Zhang, C. F.; Ouyang, J. Y.; Hao, Y. Interface Studies of the Planar Heterojunction Perovskite Solar Cells, *Sol. Energy Mater. Sol. Cells* **2016**, *157*, 783–790.
39. Lin, Y. Z.; Chen, B.; Fang, Y. J.; Zhao, J. J.; Bao, C. X.; Yu, Z. H.; Deng, Y. H.; Rudd, P. N.; Yan, Y. F.; Yuan, Y. B.; Huang, J. S. Excess Charge-Carrier Induced Instability of Hybrid Perovskites, *Nat. Commun.* 2018, 9, 4981.
40. Yuan, S.; Zheng, X. P.; Shen, W. S.; Liu, J. K.; Cui, L. S.; Zhang, C. C.; Tian, Q. S.; Wu, J. J.; Zhou, Y. H.; Wang, X. D.; Wang, Z. K.; Han, P. G.; Luther, J. M.; Osman M. Bakr, O. M.; Liao, L. S. Overcoming Degradation Pathways to Achieve Stable Blue Perovskite Light-Emitting Diodes, *ACS Energy Lett.* **2022**, *7*, 1348−1354.
41. Cheng, T.; Tumen-Ulzii, G.; Klotz, D.; Watanabe, S.; Matsushima, T.; Adachi, C. Ion Migration-Induced Degradation and Efficiency Roll-off in Quasi- 2D Perovskite Light-Emitting Diodes, *ACS Appl. Mater. Interfaces* **2020**, *12*, 33004−33013.
42. Li, N.; Song, S.; Jia, Y. H.; Dong, Y. F.; Xie, F. Y.; Wang, L. D.; Tao, S. X.; Zhao, N. Stabilizing Perovskite Light-Emitting Diodes by Incorporation of Binary Alkali Cations, *Adv. Mater.* **2020**, *32*, 1907786.
43. Zhang, T.; Hu, C.; Yang, S. H. Ion Migration: A "Double-Edged Sword" for Halide-Perovskite-Based Electronic Devices, *Small Methods* **2020**, *4*, 1900552.
44. Yu, C.; Zhang, H. J.; Wang, P.; Wang, H.; Li, T.; Zhang, X.; Cheng, S. L.; Guo, C. H. Gao, C.; Liu, D.; Wang, T. Enhanced Effciency and Stability of Quasi-2D Perovskite Light-Emitting Diodes with Crosslinkable Alkenyl Amine Cations, *Adv. Opt. Mater.* **2021**, *9*, 2101475.
45. Guo, B. B.; Lai, R. C.; Jiang, S. J.; Zhou, L. M.; Ren, Z. X.; Lian, Y. X.; Li, P. Y.; Cao, X. H.; Xing, S. Y.; Wang, Y. X.; Li, W. W.; Zou, C.; Chen, M. Y.; Hong, Z. J.; Li, C.; Zhao, B. D.; Di, D. W.; Ultrastable near-infrared perovskite light- emitting diodes, *Nat. Photon.* 2022, *16*, 637-643.

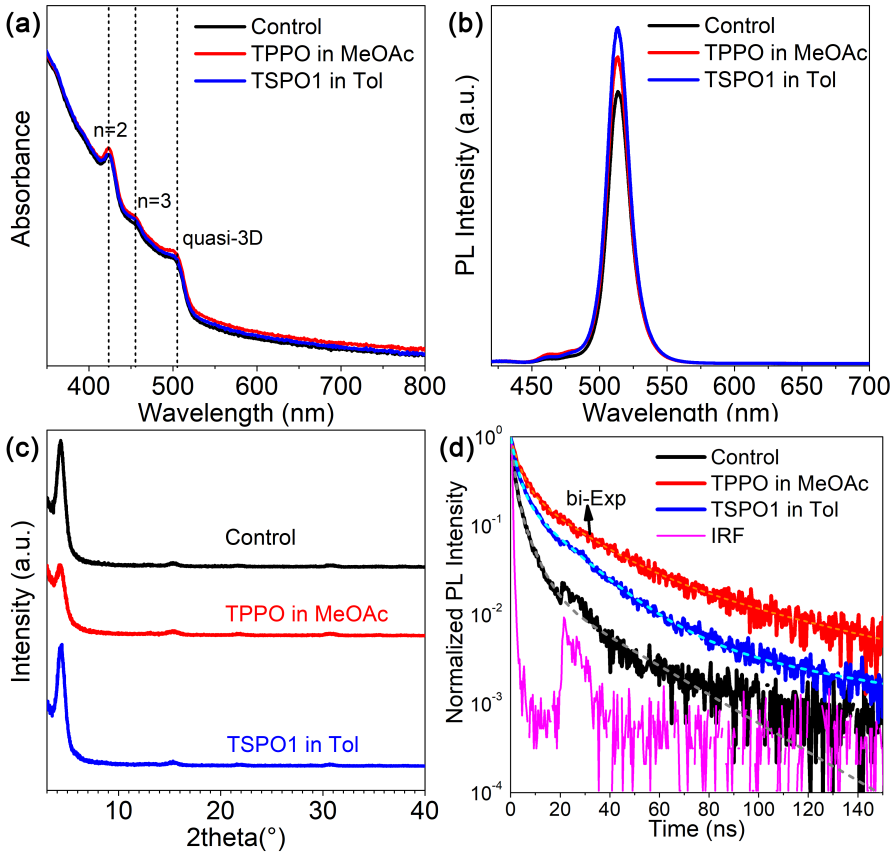

Figure 1. a) Absorption spectra, b) PL spectra, c) XRD patterns, and d) PL decay traces of HDA-DDA perovskite films with different passivation. Inset in panel (c) shows magnified 002 peak, and instrument response function (IRF) of the TCSPC system is also shown in panel d.

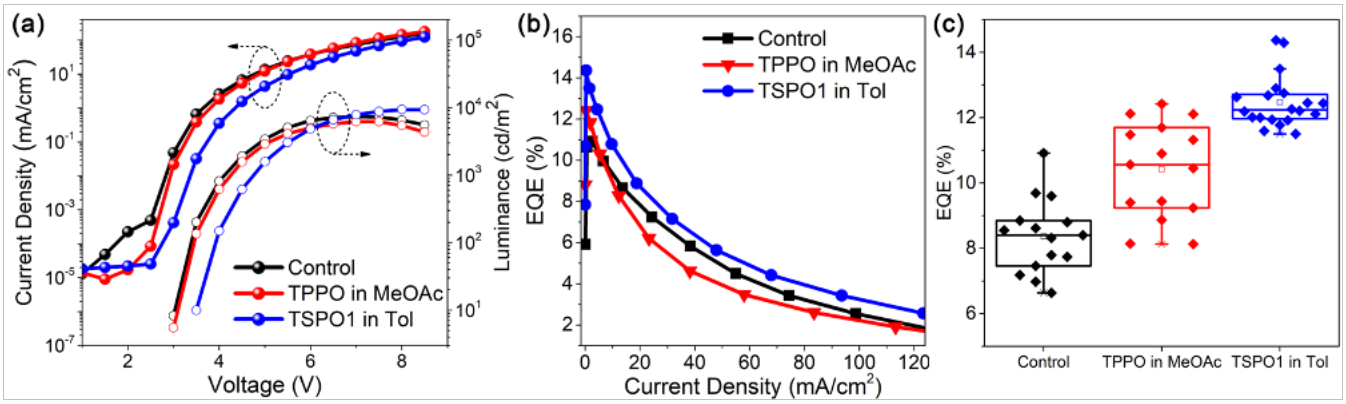

Figure 2 a) J-V-L curve b) EQE vs. current density c) EQE box plot for different passivation.

Table 1. Device performance and operational stability parameters of LEDs with and without passivation. CE denotes current efficiency.

Sample	Max EQE (%)	Max CE (cd/A)	Max Luminance (cd/m^2)	T_{50} (min)	Average EQE (%)	Average Luminance (cd/m^2)	Number of devices
Control	10.9	31.4	7349	105	8.4±1.1	6385±704	15
TPPO in MeOAc	12.4	35.3	7687	42	10.4±1.5	6137±613	15
TPPO in Tol	11.0	32.1	8376	83	9.9±0.8	7901±687	15
TSPO1 in MeOAc	11.9	32.8	9311	180	10.9±0.8	8473±571	15
TSPO1 in Tol	14.4	42.1	9363	341	12.5±0.8	7528±719	20
MeOAc	10.9	30.9	8099	86	9.4±0.7	7300±1077	15
Tol	10.3	29.9	8301	98	7.7±1.4	6670±990	15
0.5M TPPO in MeOAc	12.7	36.3	8103	63	11.3±1.1	6610±722	15

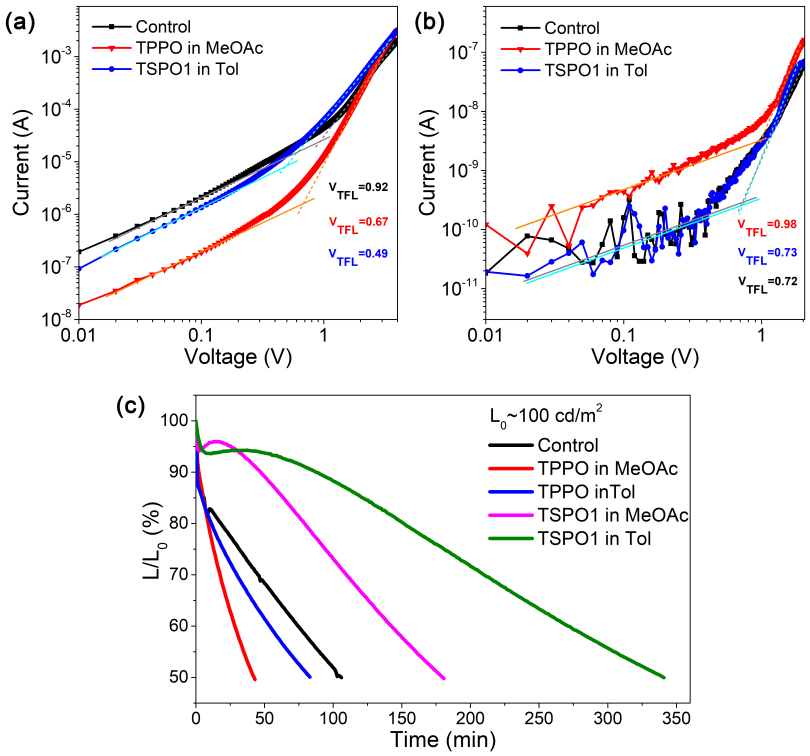

Figure 3. SCLC curves for devices with different passivation for a) hole-only devices (device architecture ITO / 2PACz / TFB / perovskites / TFB / MoO_3 / Al) b) electron-only devices (device architecture ITO / ZnMgO / perovskites / TPBi / Liq / Al); c) Relative luminance vs. time.

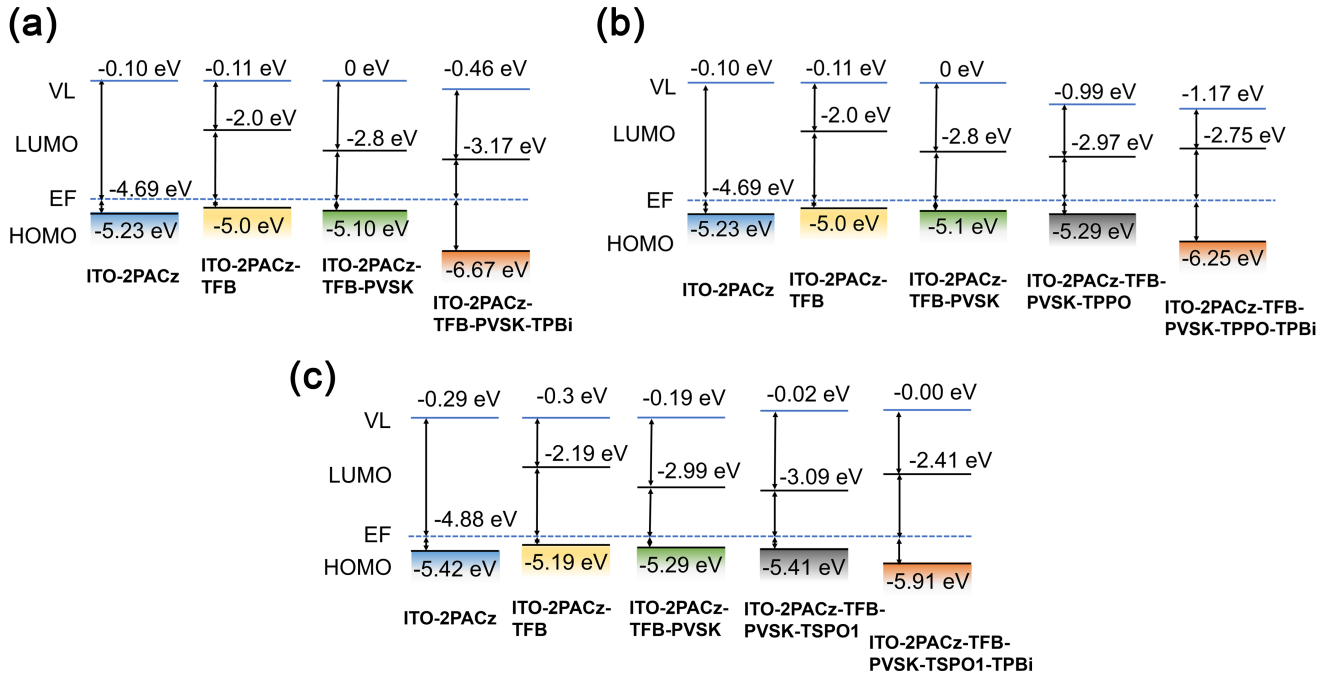

Figure 4. Schematic diagram of energy level alignments from UPS measurements: a) Control, b) TPPO in MeOAc, and c) TSPO1 in Tol.

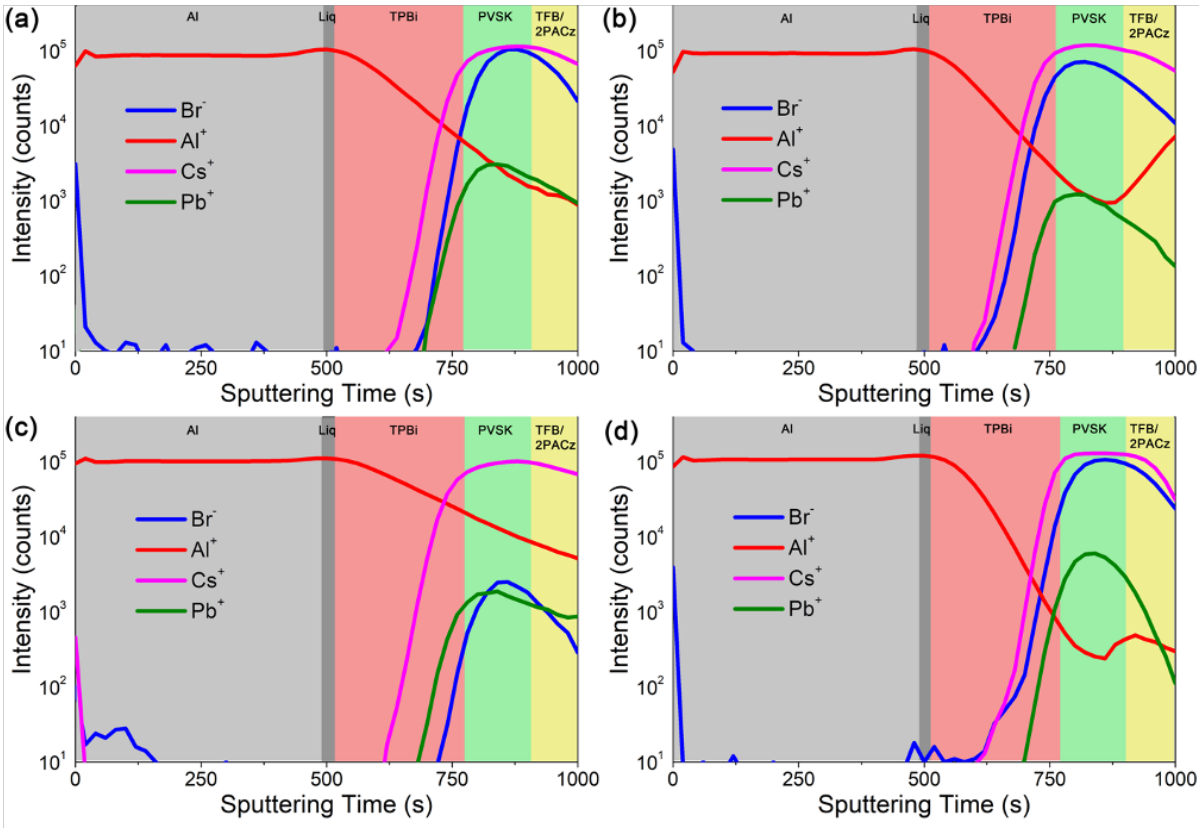

Figure 5. SIMS ion profiles for a), b) fresh and aged TPPO-passivated devices and c,d) fresh and aged TSPO1-passivated devices.

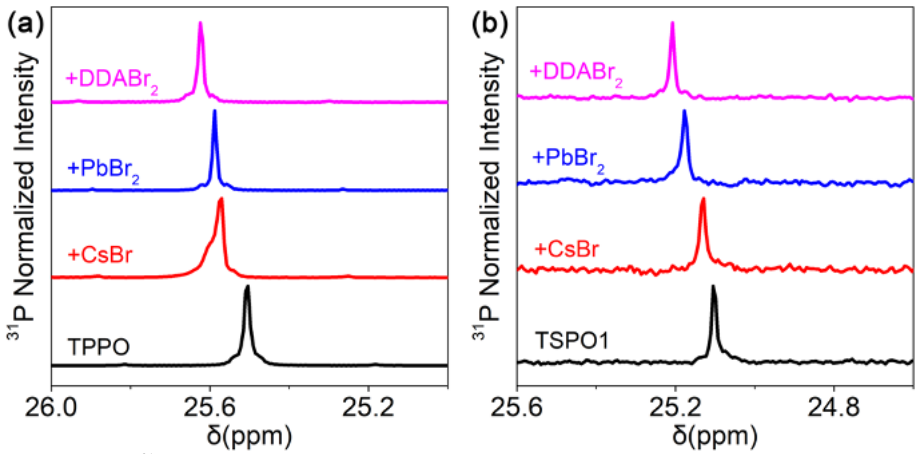

Figure 6. NMR ^{31}P spectra of passivating molecule and its mixtures with perovskite precursors for a) TPPO and b) TSPO1.

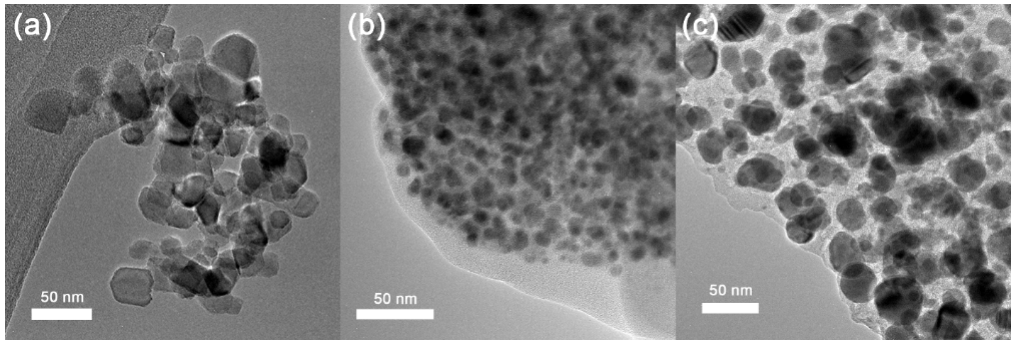

Figure 7. TEM images of perovskite samples a) Control, b) TPPO in MeOAc, and c) TSPO1 in Tol.

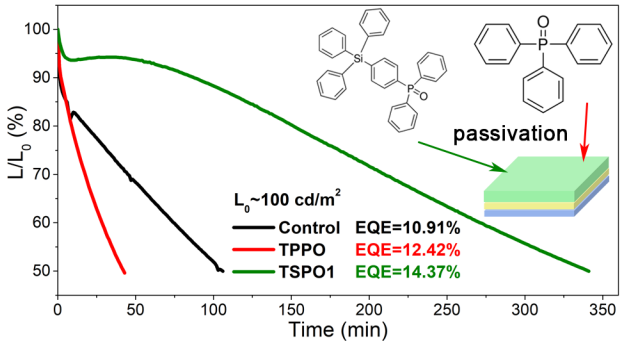
100
90
80
70
60
50
L/L0 (%)
0
50
100
150
200
250
300
350
Time (min)
passivation
L0~100 cd/m2
Control EQE=10.91%
TPPO EQE=12.42%
TSPO1 EQE=14.37%